NASA TECHNICAL MEMORANDUM

NASA TM-78851

NASA TM-78851

THE USE OF AN ION-BEAM SOURCE TO ALTER THE SURFACE MORPHOLOGY OF BIOLOGICAL IMPLANT MATERIALS

by A. J. Weigand
Lewis Research Center
Cleveland, Ohio 44135

TECHNICAL PAPER to be presented at the
Society for Biomaterials Conference
San Antonio, Texas, April 29-May 2, 1978

THE USE OF AN ION-BEAM SOURCE TO ALTER THE SURFACE MORPHOLOGY OF BIOLOGICAL IMPLANT MATERIALS

by A. J. Weigand

National Aeronautics and Space Administration
Lewis Research Center
Cleveland, Ohio 44135

E-9573

ABSTRACT

An electron-bombardment, ion-thruster was used as a neutralized-ion-beam sputtering source to texture the surfaces of biological implant materials. The materials investigated included 316 stainless steel; titanium-6% aluminum, 4% vanadium; cobalt-20% chromium, 15% tungsten; cobalt-35% nickel, 20% chromium, 10% molybdenum; polytetrafluoroethylene; polyoxymethylene; polyethylene; silicone and polyurethane copolymer; 32%-carbon-impregnated polyolefin; segmented polyurethane; silicone rubber; and alumina. Scanning electron microscopy was used to determine surface morphology changes of all materials after ion-texturing. Electron spectroscopy for chemical analysis (ESCA) was used to determine the effects of ion-texturing on the surface chemical composition of some polymers. Liquid contact angle data were obtained for ion-textured and untextured polymer samples. Results of tensile and fatigue tests of ion-textured metal alloys are presented. Preliminary data of tissue response to ion-textured surfaces of some metals, polytetrafluoroethylene, alumina, and segmented polyurethane have been obtained.

INTRODUCTION

One factor which affects the biological tissue response to an implant material is the surface morphology of the material (refs. 1 and 2).

STAR Category 23

Most surface morphologies that have been investigated have a distribution of surface pore sizes (vitreous carbon (ref. 3), porous polyolefin (ref. 4)), which may cause nonuniform tissue response to various parts of the implant. Pores too small will not allow cell ingrowth. Other pores that interconnect too far under the surface will allow tissue ingrowth without proper nutrition causing inflammation and, if severe enough, necrosis. A technique which uses technology developed from the National Aeronautics and Space Administration's electric propulsion program has been used to obtain controlled surface morphologies with well defined dimensions (ref. 5). By using implants with known surface roughnesses a systematic investigation can be performed to evaluate the tissue response to surface morphology. An optimum implant surface texture for bone, soft tissue, or thrombus attachment can be deduced from in vivo tests of implants with controlled, precise surface morphologies.

An electron-bombardment, ion thruster has been used as a neutralized-ion-beam source to modify surface morphology (ref. 6). The beam of directed, energetic ions, produced by the ion source, can alter the surface the surface morphology of many materials. When an energetic ion strikes the surface of a material (target), one or more atoms, molecules, or fragments of molecules may be removed. This process is called sputtering or ion-texturing (ref. 7). The rate at which the target material can be sputtered depends on many factors including energy of the incident ion, the rate at which the ions strike the target per unit target area (current density), and the melting or decomposition temperature of the target (ref. 8). By adjusting the ion energy and current density of the ion beam, appropriate surface modifications can be obtained without risk of target material melting or bulk decomposition.

A given ion source operating condition results in a certain repeatable surface morphology for each biological implant material (biomaterial). Metals and ceramics generally can be sputtered at high ion-beam energies, high current densities, and high surface temperatures. Metals sometimes require the use of a sputter resistant material deposited on the surface (refs. 9 and 10) to obtain a desired surface micro-

structure. The average separation between surface microstructures may range from less than 1 to 10 μm or more, and the average height of these features may range from less than 1 to 10 μm or more. Polymers generally require low ion beam energies, low current densities, and low surface temperatures to obtain a desired surface microstructure (average surface feature separations of 1 to 10 μm or more and an average height ranging from 1 to 100 μm).

To obtain larger surface roughnesses a screen mesh may be superimposed on the biomaterial during sputtering. The screen will prevent the sputtering of material directly beneath it, resulting in a surface with an array of pores of constant dimension. By varying the size of the screen apertures and the ion-texturing duration, different surface pit dimensions can be obtained. The limiting factor that determines the maximum pit depth is the screen thickness.

To determine the range of application and limitations of ion-texturing of biomaterials, an investigation of a variety of biomaterials (metals, ceramics, and polymers) was undertaken. The materials included 316 stainless steel; titanium-6% aluminum, 4% vanadium (Ti-6, 4); cobalt-20% chromium, 15% tungsten (Haynes 25); cobalt-35% nickel, 20% chromium, 10% molybdenum (MP35N); polytetrafluoroethylene (PTFE); polyoxymethylene (Delrin); carbon-impregnated (32%) polyolefin; segmented polyurethane (Biomer); polyethylene; copolymer of silicone and polyurethane (Avcothane); and silicone rubber (Silastic). Surface morphologies of ion-textured surfaces were documented using a scanning electron microscope (SEM). Electron spectroscopy for chemical analysis (ESCA) was used to determine changes in the surface (to approximately 10Å into the surface) chemical composition for some polymers. Water contact angle data for ion-textured and untextured polymers were used as an indicator of surface energy. The tensile properties of ion-textured Haynes 25 and 316 stainless steel and the fatigue properties of ion-textured Ti-6, 4 and 316 stainless steel were also determined. These tests were performed to determine if the micron and submicron surface topography which results from ion-

texturing enhances microcracks. If the probability of microcracks were increased, then the mechanical properties of the materials would be degraded.

Preliminary tissue response data of ion-textured samples have been obtained. Argon-ion-textured Biomer samples have been implanted in canine arteries (ref. 5). Ion-textured PTFE; 316 stainless steel; Haynes 25; MP35N; Ti-6, 4; and alumina have been implanted in soft tissue of rats (ref. 11). Ion-textured percutaneous connectors made of 316 stainless steel and PTFE were implanted in the dorsal dermis of cats. The results of these tests will be briefly discussed.

APPARATUS AND PROCEDURE

All ion sources used at Lewis Research Center and most ion sources in general are cylindrical in design and are typically classified according to their beam diameters (ref. 12). An 8-cm diameter ion source utilizing argon and nitrogen as the working gas was used for all the data reported herein. A 30-cm diameter ion source has also been developed at Lewis (ref. 13). Both ion sources can operate with any of the inert gases, nitrogen, freons, and other gases. These ion sources operate in a vacuum system with pressures ranging from 1.3×10^{-3} to 4×10^{-4} pascals (1×10^{-5} to 3×10^{-7} torr).

A schematic drawing of an 8-cm diameter ion source is shown in figure 1. The basic design of the ion source includes a ribbon cathode which, when heated, is the source of bombarding electrons used to ionize the working gas. The cathode is made of a triple-strand of 0.5 mm (0.020 in.) diameter, tantalum wire which is coated with a low-work-function material (BaO). The BaO aids in the electron emission process. The electron emission is controlled by the amount of power applied to the cathode filament. The discharge chamber is the volume in which the cathode electrons ionize the working gas atoms. A concentric-cylinder anode, operating at approximately +40 volts higher

potential than the cathode, is used to attract the electrons. A magnetic field, provided by six to eight 0.6 cm (0.25 in.) diameter permanent bar magnets equally spaced around the ion source, increases the bombarding electron path length through the discharge chamber. By extending the path length, the probability of ionization increases. The multiple-aperture ion extraction system consists of two grids with concentric, circular holes (ref. 14). The screen grid (adjacent to the discharge chamber) operates at a positive high voltage (300 to 2000 volts), while the accelerator grid operates at a negative voltage (-200 to -1000 volts). A neutralizer, which for this ion source is a heated loop of double-strand, tantalum wire coated with BaO, provides electrons to neutralize the extracted ion beam. There is very little (approximately 1%) re-combination of ions and electrons. This directed, slightly divergent, neutralized ion beam can then be used to sputter target material. Ion current densities from less than 0.1 to 1 mA/cm^2 are produced by the 8-cm diameter ion source. The maximum target area over which the ion current density is uniform (within 15% of maximum) is 12×12 cm at a distance of 100 cm (39 in.) from the accelerator grid plane of an 8-cm diameter ion source.

This ion source is extremely easy to operate. The operator first turns on the cathode and neutralizer filaments. When they are heated to the proper level, the working gas flow is started. The flow can be regulated by a needle value. The anode voltage is activated and a discharge is obtained. The two grid voltages are activated simultaneously which results in an ion beam. The screen grid voltage controls the ion beam energy. The ion beam current density is regulated by the anode current.

The target is usually centered on the ion beam axis. The target may be placed perpendicular to this axis or at an oblique angle depending on the application (refs. 7 and 15). Metals and ceramics are usually 10 cm from the ion source, and polymers are 20 cm away. Figure 2 illustrates the ion-texturing techniques used to generate various surface morphologies. Ion-sputtering (fig. 2(a)) is used to generate "natural" textures on polymers, ceramics, and some metal alloys.

Ion-machining (fig. 2(b)) uses a mask to produce a given surface topography. For a 20 cm ion-source-to-target distance it is important to have the mask no more than 100 μm (0.004 in.) from the target surface to insure precise definition of the mask geometry onto the target. All masks used in this study were made of nickel and derived from a commercially available electroform process. Each mask had an array of square apertures. All references to screen sizes will denote the width of the aperture. Therefore, a 158 μm screen will denote an array of holes of which each is 158×158 μm.

Figure 2(c) shows the arrangement used to generate surface textures on metals. A low-sputtering-yield, seed material is located in the proximity of the target and usually at a 30^{o}-45^{o} angle with respect to the ion beam axis. The ion beam simultaneously sputters both the target and seed material. Some of the seed material is deposited on the target surface. Because the seed material has a low sputtering yield, each atom will prevent sputtering of target material behind it (ref. 16). By adjusting the seed arrival rate, target temperature, and ion beam power, a variety of surface textures can be obtained (refs. 8 and 9).

RESULTS

Effect of Ion-Texturing on Surface Morphology

Sputtering Rate

Table I lists the ion beam energy, ion current density, distance between ion source and biomaterial, and average sputtering rate at the given operating conditions for each of the biomaterials investigated. The sputtering rate was determined by measuring the depth of the pits after sputtering a material that had a screen superimposed. SEM micrographs of a cross sectional view showing the pit depth were used.

PTFE (6 μm/hr) and Delrin (5 μm/hr) have the highest sputtering rates of all materials tested. The sputtering rates listed are close to the maximum rates capable for each material without causing thermal degradation except PTFE and Avcothane. Sputtering rates as high as 100 μm/hr have been obtained with PTFE at Lewis. Avcothane was not

tested at a ion beam current density comparable to the ion beam current density of the other polymers.

The sputtering rates for the metals (except MP35N which was not tested at a high ion current density) and alumina are representative of rates when using the 8-cm diameter ion source. These sputtering rates can be increased if a 30-cm diameter ion source, which is capable of producing higher ion current densities, is used.

Scanning electron micrographs were taken of each ion-textured surface. Figures 3 to 9 show the results of ion-texturing polymers; figures 10 to 13, metals; and figure 14, alumina. The polymer photomicrographs were taken of surfaces that did not have a screen superimposed during sputtering, although polymers have been successfully sputtered with a screen superimposed. The metals and ceramic are shown after sputtering both with and without a superimposed screen. Each material has a unique surface morphology which is reproducible using the same operating conditions.

Water Contact Angle of Polymers

Deionized water droplets of uniform size (3 mm (0.12 in.) diameter) were placed on the surface of each ion-textured and untextured polymer. Photographs were taken within 30 seconds after the droplet was placed on the surface. The contact angle (between the solid surface through the liquid to a tangent taken from the liquid-solid interface) was measured from the photographs to within ±5 degrees of the stated value. The contact angle is inversely related to the surface energy. Generally, tissue attaches (wets) more easily to material with a high surface energy (low contact angle). However, the ultimate test for tissue attachment is implantation.

The contact angle data of water on nitrogen- and argon-ion textured and untextured polymers are listed in table II. The surface morphology of nitrogen-ion-textured samples are not identical to the surface morphology of argon-ion-textured samples. However, the general topography is similar, that is, the cones on PTFE (fig. 3), the lack of micro-

meter size roughness on Silastic (fig. 9) and polyethylene (fig. 4), and the "wormy" structure on carbon-impregnated polyolefin (fig. 6).

The water contact angle for nitrogen-ion-textured surfaces indicates that the angle does not change when Biomer and Delrin are ion-textured. PTFE, carbon-impregnated polyolefin, and polyethylene show increases in the contact angle after ion-texturing. Avcothane and Silastic are the only materials that show a decrease in the contact angle of the nitrogen-ion-textured surface compared to the untextured surface.

The contact angle of water on an argon-ion-textured Biomer and Silastic samples were approximately the same as the contact angle of water on the untextured samples. All other polymers had larger contact angles after ion-texturing. These changes in contact angle for both nitrogen- and argon-ion-textured surfaces are the probable result of a combination of the effects of changes in surface topography (ref. 17) and surface chemistry.

Surface Chemical Composition of Polymers

To further characterize the effect of ion-texturing on polymers, electron spectroscopy for chemical analysis (ESCA), also known as X-ray photoelectron spectroscopy (XPS), was used to determine surface chemical composition changes that may occur due to ion-texturing. Both nitrogen- and argon-ion-textured surfaces were compared to untextured surfaces. This analysis was performed by Physical Electronics Industries, Inc., Eden Prairie, Minnesota. The major changes in chemical composition of each polymer will be discussed.

The argon-ion-textured surface of PTFE shows the presence of oxygen functionalities (ref. 18). The particular sample used for analysis did appear (SEM observation) to show signs of overheating (cones not peaked, but bent downward and jagged) which might result in the introduction of oxygen functionalities. This argument seems volid since the analysis of a nitrogen-ion-textured surface shows an almost complete absence of oxygen functionalities. This result has been reported for low energy R-F discharge sputtering (ref. 19). It appears possible to ion-

texture PTFE and produce a surface that is chemically similar to the original surface. It is also possible that the material which is sputtered from the surface can be deposited on another surface and should have properties similar to PTFE (clear, nonconducting, and composed of shorter chained $(-CF_2-)_n$). For nitrogen- and argon-ion-textured samples of Biomer, 32% carbon impregnated polyolefin, and Silastic the C_{1s} peak increases compared to the untextured samples. This result indicates a carbon enhancement on the surface. Polyethylene samples that were nitrogen- argon-ion-textured showed an oxygen enhancement on the surface. Nitrogen-ion-textured Avcothane samples showed no change in surface composition, and for argon-ion-textured Avcothane samples there is an enhancement of carbon.

Mechanical Properties of Metal Alloys

Standard 0.29 cm (0.11 in.) diameter tensile samples of Haynes 25 and 316 stainless steel and standard 0.6 cm (Ti-6, 4) and 1.1 cm (316 stainless steel) diameter fatigue samples were ion-textured around the entire circumference (ref. 20). The microstructure on these samples was similar to the microstructure shown in figures 10(a), 11(a), and 12(a). One Ti-6, 4 fatigue sample was ion machined with a 158 μm nickel mesh superimposed. The resulting 140×140 μm deep pits covered one quarter of the sample surface area.

Examination of the effects of an ion-textured surface on the mechanical properties (ultimate strength, yield strength, and fatigue strength) of representative biological implant materials revealed very little degradation of the properties. The average ultimate strength and average yield strength of Co-20%Cr-15%W was the same (within 5%) for ion-textured and untextured samples. The 316 stainless steel samples that were tensile tested revealed that the average ultimate strength was unchanged (within 4%) after ion-texturing. The average yield strength increased 20% after ion-texturing but this increase may be due to the lack of a statistically significant number of samples rather than a change in the yield strength.

Fatigue specimens of Ti-6%Al, 4%V and 316 stainless steel that were ion-textured showed no change in fatigue strength when compared to untextured samples. The fatigue strength of a Ti-6%Al, 4%V sample that was ion-textured with a 158×158 μm pore Ni mesh covering its surface was 30 percent lower than the untextured fatigue strength for a load of $\pm 4.5 \times 10^8$ N/m^2 ($\pm 66.2 \times 10^3$ psi).

Tissue Response Data for Ion-Textured Implants

Argon-ion-textured Biomer samples (3×5×0.25 mm) were implanted into canine arteries (ref. 5). The initial thrombus growth (after 1 hr) was accelerated when compared to the growth on untextured samples. However, the final thrombus thickness was the same for both ion-textured and untextured samples.

Xenon-ion-textured titanium and MP35N dental implants (endosteal blade vent implants) were tested in beagles (ref. 21). Preliminary results indicate a high ion-textured implant success rate (6 out of 7) and a minimal tissue inflamatory or foreign body response. There was close adaptation of interfacial tissue with the implant surface.

Flat 1×3 cm implants made of PTFE, alumina, Haynes 25, Ti-6, 4, and 316 stainless steel were ion-machined with different screen aperture sizes and for different durations. Table III lists the materials, the aperture widths, and the aperture width to aperture depth ratio. These implants were tested in dorsal subcutaneous soft tissue of rats (ref. 11). After an implantation duration of 6 weeks, the implants were tested for mechanical attachment by means of a "pull out" test. An instron test instrument was used to measure the shear strength of the tissue-implant interface. Table III lists the maximum load needed to separate tissue from each implant. These results indicate an increase in the tissue attachment to ion-textured implants compared to untextured samples (nominal load, 5 g). There was no evidence of an inflammatory cell response in the tissue surrounding the implants. The fibroblasts in the capsule adjacent to the implant did, however, suggest a more active response.

CONCLUDING REMARKS

It has been demonstrated that an electron-bombardment ion source has the ability to produce well defined, reproducible surface morphologies on polymers, metals, and a ceramic. For some materials average surface roughnesses ranging from less than 1 μm to more than 100 μm have been achieved. By using screen masks with apertures between 20 and 158 μm, surfaces with arrays of uniform topography have been obtained. Since the surface chemistry of ion-textured biomaterials has been determined, a programmatic study varying the surface morphology in a controlled, precise way can be undertaken.

Documentation of the effect of ion-texturing on eleven biomaterials has revealed the following results.

High sputtering rates have been obtained for polytetrafluoroethylene and polyoxymethylene. Metals and ceramics in compansion have lower sputtering rates. Because of the temperature constraints (decomposition) of polyethylene, carbon-impregnated polyolefin, silicone rubber, segmented polyurethane, and copolymer of silicone and polyurethane, these materials have low sputtering rates.

The water contact angle measurements of argon-ion-textured segmented polyurethane and silicon rubber was approximately the same as the contact angle measurements of water on untextured samples. Polyethylene, copolymer of silicon and polyurethane, carbon-impregnated polyolefin, polytetrafluoroethylene, and polyoxymethylene samples that were textured with an argon-ion beam and larger water contact angles.

Nitrogen-ion-textured segmented polyurethane and polyoxymethylene showed no change in water contact angle when compared to untextured sample data. Polytetrafluoroethylene, carbon-impregnated polyolefin, and polyethylene samples show an increase in the contact angle after ion-texturing. Copolymer of silicone and polyurethane and silicone rubber nitrogen-ion-textured samples show a decrease in water contact angle compared to untextured sample data.

X-ray photoelectron spectroscopic examination of an overheated polytetrafluoroethylene ion-textured sample indicated an increase in oxygen functionalities. A polytetrafluoroethylene nitrogen-ion textured sample and segmented polyurethane, carbon-impregnated polyolefin, silicone rubber, and copolymer of silicone and polyurethane nitrogen- and argon-ion-textured samples were shown to have a carbon enhancement on the surface compared to untextured sample data. Polyethylene samples textured with nitrogen- and argon-ions had an increase of oxygen on the surface.

It has been demonstrated that ion-texturing of metals does not degrade the mechanical properties.

The ultimate strength, yield strength, and fatigue strength of cobalt-20% chromium, 15% tungsten and 316 stainless steel tensile samples was unchanged after ion-texturing. Fatigue samples of titanium-6% aluminum, 4% vanadium and 316 stainless steel that were ion-textured showed no change in fatigue strength when compared to untextured samples. The fatigue strength of a titanium-6% aluminum, 4% vanadium sample that was ion-textured with a 158 μm Ni screen covering its surface was 30 percent lower than the untextured fatigue strength for a load of $\pm 4.5 \times 10^8$ N/m^2 ($\pm 66.2 \times 10^3$ psi).

Initial thrombus growth of an ion-textured segmented polyurethane implant was accelerated when compared to the thrombus growth of untextured samples. However, the final thrombus thickness was the same for both ion-textured and untextured samples.

Ion-textured dental implants had a high success rate (6 out of 7) and a minimal tissue inflammatory or foreign body response. There was close adaptation of interfacial tissue with the implant surface.

Soft tissue samples of ion-machined polytetrafluoroethylene; alumina; cobalt-20% chormium, 15% tungsten; titanium-6% aluminum, 4% vanadium, and 316 stainless steel had an increase in tissue attachment compared to untextured samples. There was very little inflammation around the ion-textured implants.

REFERENCES

1. Szycher, M; et al.: Development and Testing of Flocking Materials. NO1-HV-3-2915-4, Thermo Electron Corp., 1977.

2. Ducheyne, P; et al.: Influence of a Functional Dynamic Loading on Bone Ingrowth into Surface Pores of Orthopedic Implants. J. Biomed. Mater. Res., vol. 11, no. 6, Nov. 1977, pp. 811-838.

3. Spector, M; Kreutner, A; and Sauer, B. W.: Scanning Electron Microscopy of the Healing Response of Porous Orthopedic and Dental Implants. Scanning Electron Microscopy, 1976, O. Johari and R. P. Becker, eds., Vol. 2, Part 5, IIT Research Institute, 1976, pp. 299-306.

4. Nose, Y.; et al.: Development and Evaluation of Cardiac Prostheses. N01-HV-4-2960-2, National Institute of Health, 1976.

5. Banks, B. A.; et al.: Potential Biomedical Applications of Ion Beam Technology. NASA TM X-73512, 1976.

6. Weigand, A. J. and Banks, B. A.: Ion-Beam-Sputter Modification of the Surface Morphology of Biological Implants. J. Vac. Sci. Technol., vol. 14, no. 1, Jan-Feb. 1977, pp. 326-331.

7. Hudson, W. R.: Nonpropulsive Applications of Ion Beams. AIAA Paper 76-1015, Nov. 1976.

8. Weigand, A. J., Meyer, M. L.; and Ling, J. S.: Scanning-Electron-Microscopy Observations and Mechanical Characteristics of Ion-Beam-Sputtered Surgical Implant Alloys. NASA TM X-3553, 1977.

9. Hudson, W. R.: Ion Beam Texturing. NASA TM X-73470, 1976.

10. Hudson, W. R.; Weigand, A. J.; and Mirtich, M. J.: Optical Properties of Ion Beam Textured Metals. NASA TM X-73598, 1977.

11. Gibbons, D. F.: Effect of Surface Texture by Ion Beam Sputtering on Implant Biocompatibility and Soft Tissue Attachment. (Case Western Reserve Univ.; NASA Grant NSG-3126.) NASA CR 135311, 1977.

12. Ion Propulsion for Spacecraft. NASA Lewis Research Center, Cleveland, Ohio, 1977.

13. Sovey, J. S.: A 30-Cm Diameter Argon Ion Source. NASA TM X-73509, 1976.

14. Rawlin, V. K.; Banks, B. A.; and Byers, D. C.: Design, Fabrication, and Operation of Dished Accelerator Grids on a 30-Cm Ion Thruster. NASA TM X-68013, 1972.

15. Hudson, W. R.; Robson, R. R.; and Sovey, J. S.: Ion-Beam Technology and Applications. NASA TM X-3517, 1977.

16. Wehner, G. K.; and Hajicek, D. J.: Cone Formation on Metal Targets During Sputtering. J. Appl. Phys., vol. 42, no. 3, Mar. 1971, pp. 1145-1149.

17. Dettre, R. H.; and Johnson, R. E., Jr.: Contact Angle Hysteresis, II. Contact Angle Measurements on Rough Surfaces. Contact Angle, Wettability, and Adhesion, Advances in Chemistry Series 43, American Chemical Society, 1964, pp. 136-144.

18. Yasuda, H.; et al.: ESCA Study of Polymer Surfaces Treated by Plasma. J. Polym. Sci., vol. 15, 1977, pp. 991-1019.

19. Moriuchi, T.; et al.: Surface Properties of Sputter Etched Fluoropolymers. Presented at the 7th International Vacuum Congress and 3rd International Conference on Solid Surfaces (Vienna), 1977, pp. 1501-1504.

20. Weigand, A. J.: Mechanical Properties of Ion Beam Textured Surgical Implant Alloys. NASA TM X-73742, 1977.

21. Babbush, C. A.: Endosteal Blade Vent Implants Modified by Ion Beam Sputtering Techniques, NASA Grant NSG 3110, 1977.

TABLE I. - SPUTTERING RATES OF BIOMATERIALS

Material	Ion beam energy, eV	Ion current density, mA/cm^2	Distance between ion source and biomaterial, cm	Average sputtering rate, $\mu m/hr$*
Polymers				
Polytetrafluoroethylene	500	0.2	20	6
Polyoxymethylene	500	.05	20	5†
32%-Carbon-impregnated polyolefin	500	.05	20	1†
Segmented polyurethane	500	.1	30	1†
Silicone rubber	500	.1	20	2†
Copolymer of silicone and polyurethane	500	.01	100	0.1
Polyethylene	300	.05	20	1†
Metals				
316 Stainless steel	2000	.2	10	3
Co-35%Ni, 20%Cr, 10%Mo	2000	.01	100	0.1
Ti-6%Al, 4%V	2000	.2	10	4
Co-20%Cr, 15%W	2000	.4	10	2
Ceramic				
Alumina	1750	.4	20	1

*Calculated from ion-texturing with screen superimposed.

†Approximately maximum sputtering rate due to thermal constraints of material.

TABLE II. - WATER CONTACT ANGLE, θ, OF ION TEXTURED AND UNTEXTURED POLYMERS

Material	Water contact angle, θ, degrees		
	Untextured surface	Argon-ion-textured surface	Nitrogen-ion-textured surface
Polytetrafluoroethylene	114	140	156
Polyoxymethylene	83	116	82
32% Carbon-impregnated polyolefin	86	97	117
Segmented polyurethane	86	81	85
Silicone rubber	113	109	98
Copolymer of silicone and polyurethane	114	126	96
Polyethylene	35	93	62

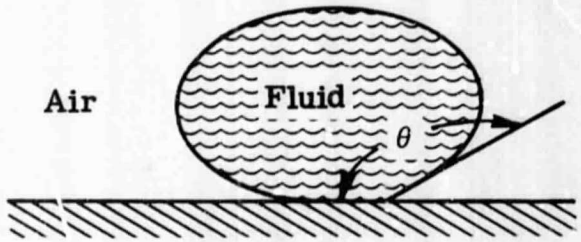

TABLE III. - MECHANICAL ATTACHMENT STRENGTHS OF ION-MACHINED BIOMATERIALS

Material	Aperture width, μm	Aperture width aperture depth	Maximum load on pull out test, g
PTFE	25 μ	0.5	40; 65
		.25	27; 36
		.16	19; 30
		.1	33; 22
PTFE	50 μ	1.0	Animal died before test completed
		.3	26; 13
		.16	140; 55
		.1	Single sample showed no attachment
Alumina	50 μ	2.0	97
Co-20%Cr, 15%W	70 μ	~3.0	110; 140; 156; 152
Titanium 6%Al-4%V	70	~3.0	98
	48	~2.0	175; 176
316 Stainless steel	70	~3.0	194; 255; 285

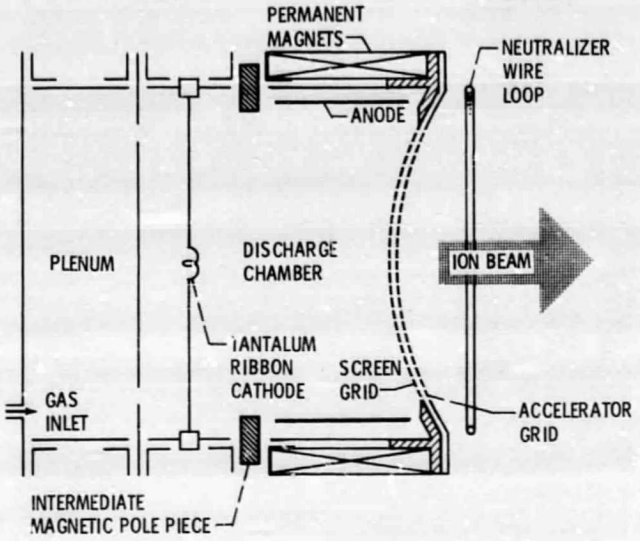

Figure 1. - Cross section of ion-beam source.

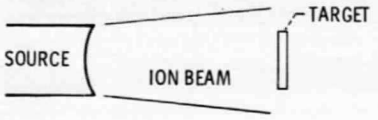

(a) ION BEAM SPUTTERING.

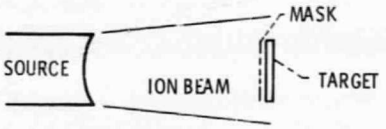

(b) ION BEAM MACHINING WITH MASK.

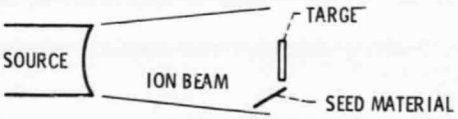

(c) ION BEAM SURFACE TEXTURING WITH SEED MATERIAL.

Figure 2. - Ion-beam sputtering techniques.

Figure 3. - Argon-ion textured polytetrafluorolthylene, 3000X.

Figure 4. - Argon-ion textured poly oxymethylene, 100X.

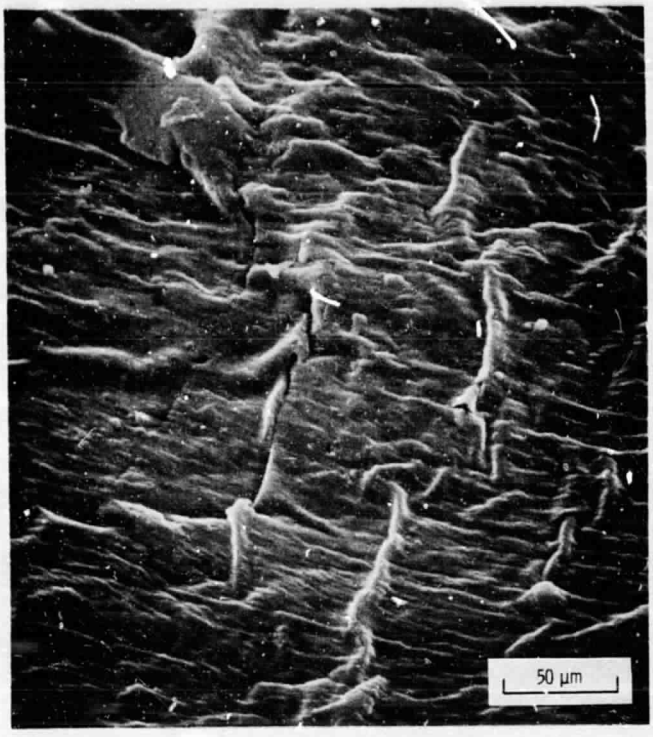

Figure 5. - Argon-ion textured polyethylene, 3000X.

E-9573

Figure 6. - Argon-ion textured 32% carbon-impregnated polyolefin, 1000X.

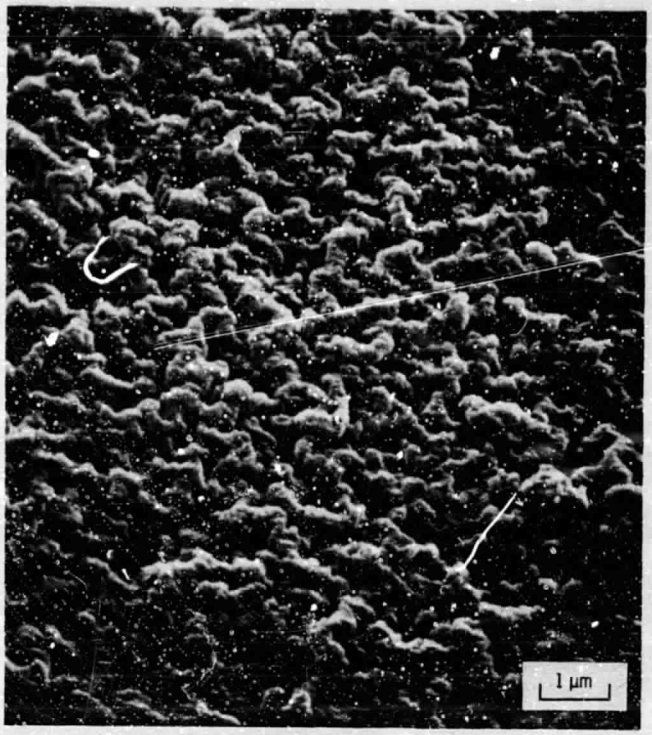

Figure 7. - Argon-ion textured segmented polyurethane, 10 000X.

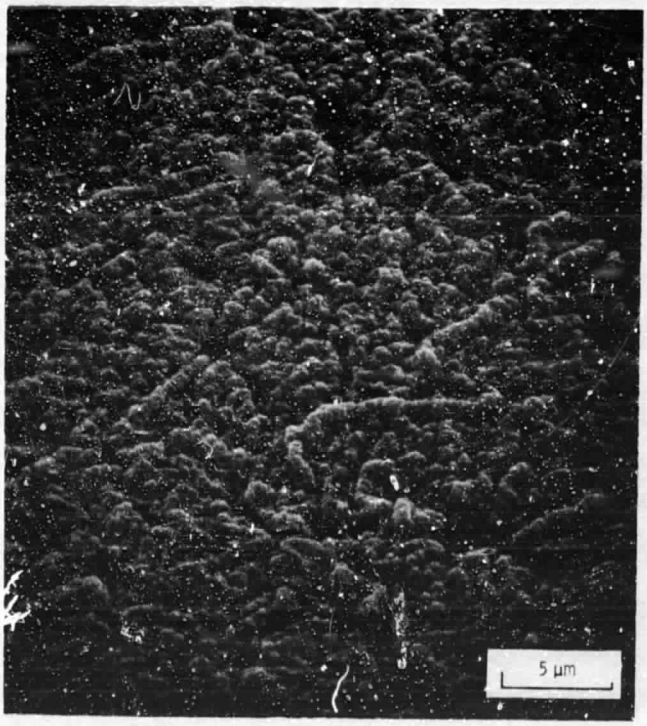

Figure 8. - Argon-ion textured copolymer of silicone and polyurethane, 3000X.

E-9573

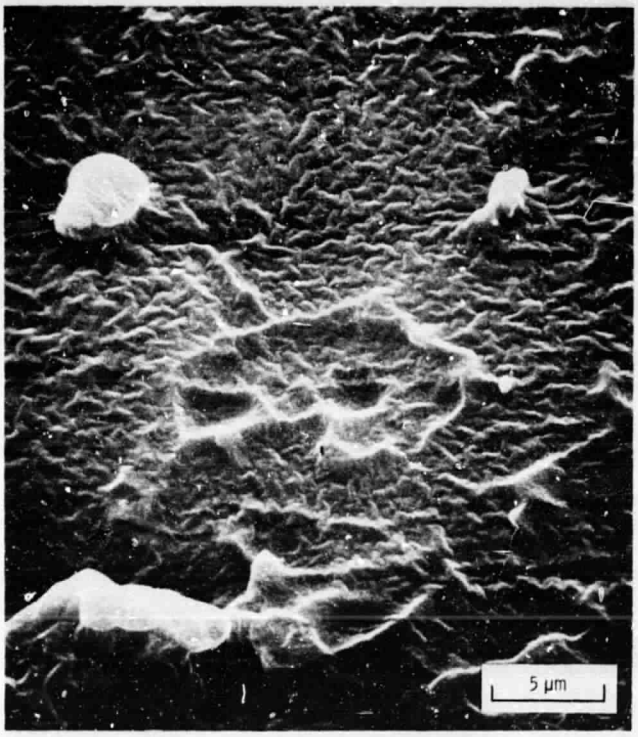

Figure 9. - Argon-ion textured silicone rubber, 3000X.

(a) NO SCRFEN, 1000X.

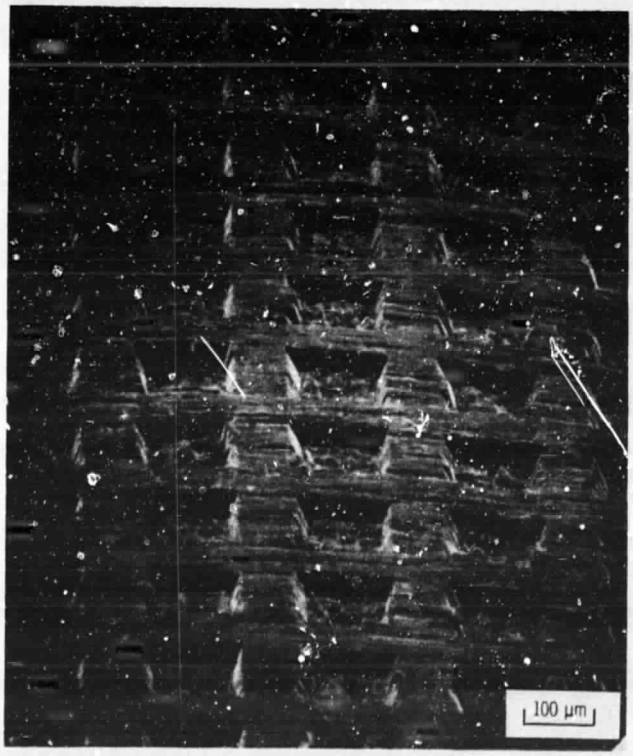

(b) 158 μm MESH SUPERIMPOSED, 100X.

Figure 10. - Argon-ion textured 316 stainless steel.

(a) NO SCREEN, 10 000X.

(b) 158 μm MESH SUPERIMPOSED, 100X.

Figure 11. - Argon-ion textured Ti-6% Al, 4% V.

(a) NO SCREEN, 3000X.

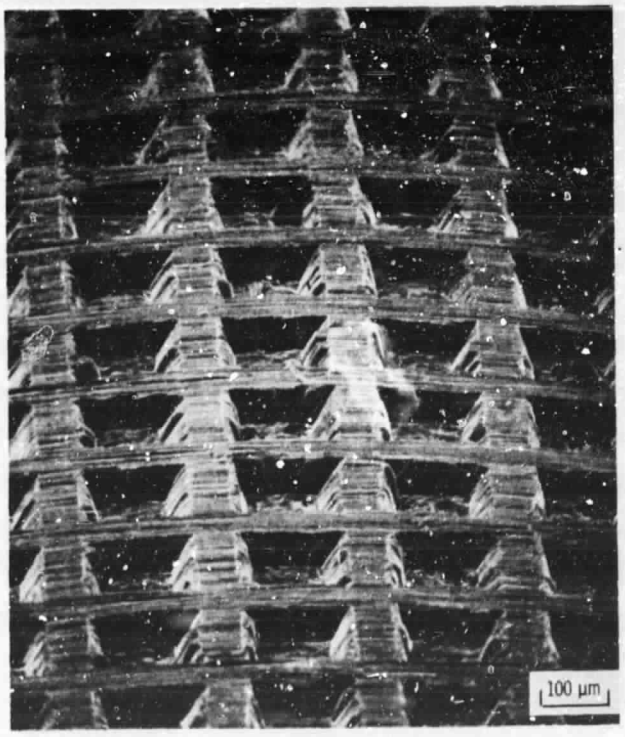

(b) 158 μm MESH SUPERIMPOSED, 100X.

Figure 12. - Argon-ion textured cobalt, 20% chromium, 15% tungsten.

(a) NO SCREEN, 1000X.

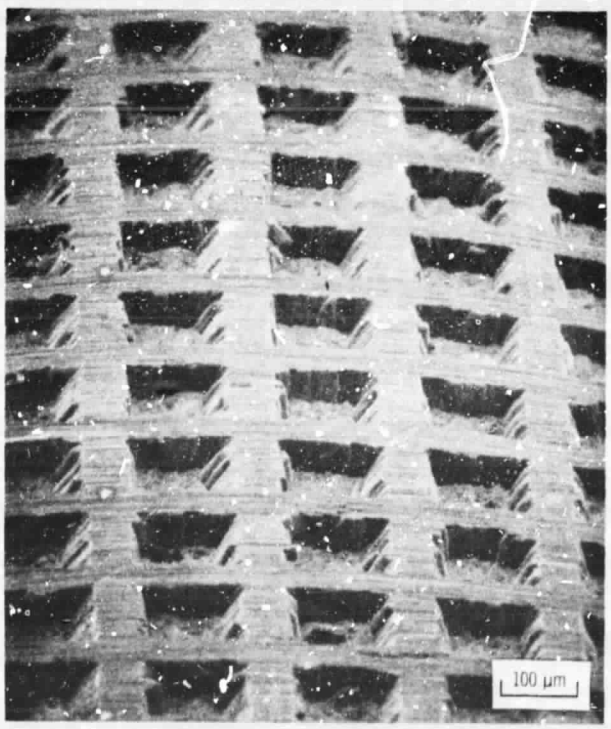

(b) 158 μm MESH SUPERIMPOSED, 100X.

Figure 13. - Argon-ion textured cobalt-35% Ni, 20% chromium, 10% molybdenum, 1000X.

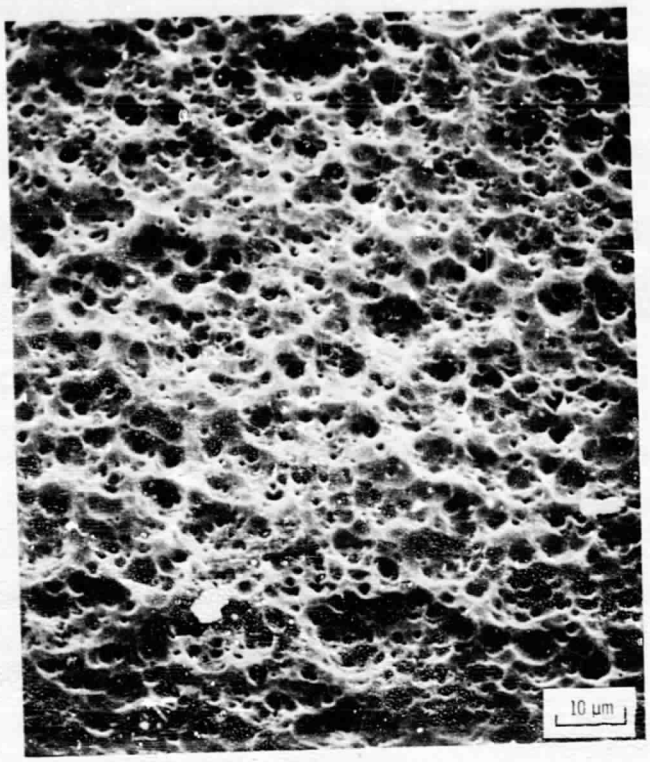

(a) NO SCREEN, 1000X.

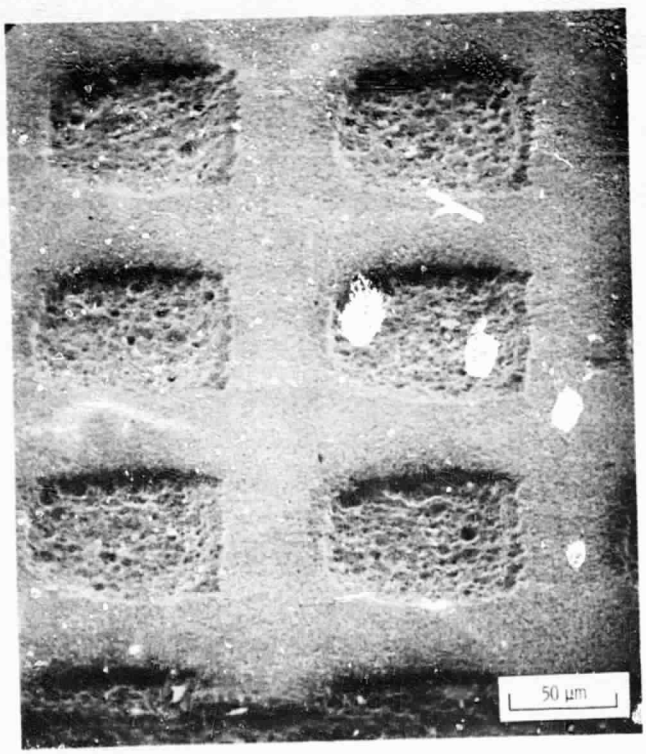

(b) 50 µm MESH SUPERIMPOSED.

Figure 14. - Argon-ion textured alumina.

NASA-Lewis